# Hydrogen-Bonding-Induced Conformational Change from J to H Aggregate in Novel Highly Fluorescent Liquid-Crystalline Perylenebisimides

B. Jancy and S. K. Asha*

*Polymer Research Group, Chemical Sciences & Technology Division, National Institute for Interdisciplinary Science and Technology (formerly Regional Research Laboratory), Thiruvananthapuram 695019, Kerala, India*

*Received September 1, 2007*

A series of highly fluorescent liquid-crystalline perylenebisimide molecules having amide or ester linkage and end-capped by phenyl, monododecyloxy phenyl, or tridodecyloxy phenyl units have been synthesized and fully characterized. The amide-functionalized series self-organized to form H type aggregates regardless of their end-capping in organic solvents like tetrahydrofuran (THF), toluene, and dichloromethane. On the other hand, only the monododecyloxy phenyl end-capped molecule in the ester series showed a tendency to self-organize with a typical J type aggregation in toluene. In both series, the highest aggregation tendency was shown by the one having monododecyloxy phenyl end-capping, with the transition temperature from aggregated to molecularly dissolved species occurring at 60 °C for the amide and 50 °C for the ester molecule. At higher concentrations in toluene, the fluorescence spectra of the monododecyloxy phenyl and tridodecyloxy phenyl terminal-substituted amide derivatives showed the formation of a new peak corresponding to excimer emission at 670 nm. Thin drop cast films of the perylenebisimide ester and amide series gave only excimer emission ~670 nm upon excitation. Thermal analysis using differential scanning calorimetry (DSC), polarized light microscopy (PLM), and powder X-ray diffraction measurements were utilized to study the liquid-crystalline (LC) characteristics of the molecules. Scanning electron micrograph (SEM) of thin drop-cast samples that were annealed in toluene showed the formation of supramolecular rods several micrometers in length, especially for the amide derivatives. The ester derivative, on the other hand, showed a leaflike morphology thus differentiating it from the amide series, which have both hydrogen bonding and $\pi-\pi$ interactions to support self-organization.

## Introduction

Perylene tetracarboxylic diimide is one of the few classes of n-type semiconducting molecule that has high thermal- and photostability. They are known to form self-organized architectures because of their inherent $\pi-\pi$ interactions. It has been shown that increased ordering of perylene molecules leads to an increase in exciton diffusion length and an improvement in charge carrier mobilities, which in turn improves the performance of devices like OLEDs and solar cells.[1,2] The solid-state packing of the perylenebisimide derivatives thus plays a very important role in improving the device performance along with their intrinsic molecular chemical and physical properties. Inducing liquid crystallinity (LC) is one way of improving organization because it promotes $\pi-\pi$ stacking, allows for dynamic reorganization, and facilitates processing in the form of thin films, which is not feasible with organic single crystals.[3–9] The organization afforded by the liquid-crystalline phase can be taken one step further by combining it with the forces of supramolecular assembly to design supramolecularly augmented LC phases with well-defined super structures. The additional stability afforded by the supramolecular forces assist in producing highly stable supramolecular liquid crystalline architectures. Among the various methods that have been adopted to bring about supramolecular self-organization, the $\pi-\pi$ interactions and hydrogen-bonding interactions are the most thoroughly studied. The introduction of amide groups into substituted benzene compounds has been known to induce and stabilize liquid crystalline phases through the formation of 1D hydrogen bonding.[7] Di- and triamide substituted benzene derivatives were shown to exhibit columnar liquid-crystalline phases.[10,11] Bis amides having trialkoxy-substituted benzene,

* Corresponding author. E-mail: asha_syamakumari@yahoo.co.in. Fax: 0091-471-2491712.

(1) Löhmannsröben, H.-G.; Langhals, H. *Appl. Phys. B* **1989**, *48*, 449–452.
(2) Liu, S. G.; Sui, G.; Cormier, R. A.; Leblanc, R. M.; Gregg, B. A. *J. Phys. Chem. B* **2002**, *106*, 1307–1315.
(3) Simpson, C. D.; Wu, J.; Watson, M. D.; Müllen, K. *J. Mater. Chem.* **2004**, *14*, 494–504.
(4) An, Z.; Yu, J.; Jones, S. C.; Barlow, S.; Yoo, S.; Domercq, B.; Prins, P.; Siebbeles, L. D. A.; Kippelen, B.; Marder, S. R. *Adv. Mater.* **2005**, *17*, 2580–2583.
(5) Syamakumari, A.; Schenning, A. P. H. J.; Meijer, E. W. *Chem.—Eur. J.* **2002**, *8*, 3353–3361.
(6) vanHerrikhuyzen, J.; Asha, S. K.; Schenning, A P. H. J.; Meijer, E. W. *J. Am. Chem. Soc.* **2004**, *126*, 10021–10027.
(7) Kato, T.; Mizoshita, N.; Kishimoto, K. *Angew. Chem,. Int. Ed.* **2006**, *45*, 38–68.
(8) Hoeben, F. J. M.; Jonkheijm, P.; Meijer, E, W.; Schenning, A. P. H. J. *Chem. Rev.* **2005**, *105*, 1491–1546.
(9) Percec, V.; Aqad, E.; Peterca, M.; Imam, M. R.; Glodde, M.; Bera, T. K.; Miura, Y.; Balagurusamy, V. S. K.; Ewbank, P. C.; Würthner, F.; Heiney, P. A. *Chem.—Eur. J.* **2007**, *13*, 3330–3345.

10.1021/cm702497y CCC: $40.75 
Published on Web 12/05/2007

which acts like a dendrimer wedge, were also shown to induce and stabilize hexagonal columnar mesophases.[12]

The number of reports on liquid-crystalline perylenebisimides without any bay substitution are only very few despite the large volume of research carried out on them.[6,13–19] Recently, there have been reports from various groups, including ours, that showed that tridodecyloxy-phenyl-substituted perylene tetracarboxylic diimides (PTCDI) can form liquid-crystalline phases.[20,21] Trialkoxy benzene moiety with long alkyl chains (e.g., dodecyloxy unit) can introduce microsegregation into the system, especially those having rigid aromatic cores like that of perylene. The nonpolar flexible alkyl chains and the rigid aromatic core make a good rigid−flexible balance that has been made use of in the design and development of perylene-based liquid crystals.[22–24] However, the tridodecyloxyphenyl substitution is generally known to quench fluorescence because of photoinduced electron transfer from the electron-rich trialkoxyphenyl group to the electron-deficient perylene core.[19,25]

Here, we report the synthesis of a family of highly luminescent liquid crystals based on n-type perylenebisimide and their aggregation behavior in solution and solid-state packing. Perylenebisimide derivatives have been studied thoroughly, especially as possible candidates for organic photovoltaic devices. Supramolecular organization in these systems can lead to well-defined pathways for electron transport, which can help improve the efficiency of devices made out of these materials. Hence, it was our aim to make use of a design strategy combining winning combinations of specific molecular interactions in the form of hydrogen bonding and $\pi-\pi$ interactions along with balancing the rigidity−flexibility ratio of the molecular shape in the development of a new series of perylenebisimide-based liquid-crystalline materials. These new molecules were designed in such a way as to address some of the fundamental questions on the self-organization and solid-state morphology of these perylenebisimide derivatives like (1) role of hydrogen bonding, (2) role of steric hindrance, (3) effect of long alkoxy terminal substituents, (4) effect of length of connecting spacer segment, etc., on the solution as well as bulk properties. We have also attempted to increase the ordering of the perylene derivatives in the presence of solvent vapors similar to the attempts reported in literature.[26,27] We also report the self-organization of these liquid-crystalline perylenebisimide derivatives into micro- and nanoaggregates whose morphology is defined by the nature of functional groups and presence or absence of long alkoxy terminal units. This is the first time that such a systematic approach has been adopted toward understanding the structural criteria that define the self-assembly process in a series of perylenebisimide derivatives.

## Experimental Section

**Materials.** Perylene-3,4,9,10-tetracarboxylicdianhydride (PTCDA), 1,6-diaminohexane, 6-aminohexanol, *N*,*N*-dimethylacetamide (DMAc), *N*-methyl pyrrolidinone (NMP), 3,4,5-trihydroxy benzoic acid, *p*-hydroxy benzoic acid, and 1-bromododecane were purchased from Sigma Aldrich and used without further purification. Zinc acetate, imidazole, benzoyl chloride, thionyl chloride, and pyridine were purchased locally and purified using standard procedures. All solvents were of AR quality and used as received.

**Instrumentation and Characterization.** $^1$H NMR spectra were recorded using 300-MHz Brucker NMR spectrophotometer in $CDCl_3$ containing small amounts of TMS as internal standard. The purity of the compounds was determined by a Shimadzu QP-2000 (GC/MS) Micromass TOF Spec 2E instrument using a nitrogen 337 nm laser (4 ns pulse). The matrix used was 2,5-dihydroxy benzoic acid dissolved in $CHCl_3$, which was spotted on MALDI target and allowed to dry before being introduced into the mass spectrometer. The purity of the oligomers was further analyzed by SEC in THF using polystyrene standards for the calibration. Waters 510 Pump connected through three series of Styragel HR columns and Waters model 2487 dual wavelength UV−vis detector was used for analyzing the samples. The flow rate of the THF was maintained as 1 mL throughout the experiments, and the sample solutions at very dilute concentrations were filtered and injected for recording the GPC chromatograms at 30 °C. Infrared spectra were recorded using a Perkin Elmer Spectrum One FT-IR spectrophotometer in the range of 4000−400 cm$^{-1}$. UV−vis spectra were recorded using a Perkin Elmer Lambda 35 UV−vis spectrometer. The emission studies were performed by a SPEX Fluorolog F112X spectrofluorimeter. The fluorescence quantum yields of the perylene derivatives were determined in toluene using Rhodamine 6G in water ($\varphi$ = 0.95) as the standard by exciting at 524 nm. The optical density at $\lambda_{524}$ was maintained at 0.1 ± 0.05 to avoid reabsorption artifacts. Thermogravimetric analysis (TGA) was performed using a TGA-50 Shimadzu thermogravimetric analyzer. Samples were run from 40 to 700 °C with a heating rate of 10 °C/min under nitrogen. DSC measurements were performed on a DSC-Perkin Elmer Pyris 6 DSC instrument at a heating rate of 10 °C/min under a nitrogen atmosphere. Typically, 2–3 mg of samples was placed in an aluminum pan, sealed properly, and scanned from 10–280 °C. The

(10) Bushey, M. L.; Hwang, A.; Stephens, P. W.; Nuckolls, C. *J. Am. Chem. Soc.* **2001**, *123*, 8157–8158.
(11) Van Gorp, J. J.; Vekemans, J. A. J. M.; Meijer, E. W. *J. Am. Chem. Soc.* **2002**, *124*, 14759–14769.
(12) Percec, V.; Ahn, C. H.; Bera, T. K.; Ungar, G.; Yeardley, D. J. P. *Chem.—Eur. J.* **1999**, *5*, 1070–1083.
(13) Cormier, R. A.; Gregg, B. A. *J. Phys. Chem. B.* **1997**, *101*, 11004–11006.
(14) Schlichting, P.; Rohr, U.; Müllen, K. *J. Mater. Chem.* **1998**, *8*, 2651–2655.
(15) Göltner, C.; Pressner, D.; Müllen, K.; Spie$\beta$, H. W. *Angew. Chem., Int. Ed.* **1993**, *32*, 1660–1662.
(16) Müller, G. R. J.; Meiners, C.; Enkelmann, V.; Geerts, Y.; Müllen, K. *J. Mater. Chem.* **1998**, *8*, 61–64.
(17) Rohr, U.; Schlichting, P.; Böhm, A.; Gross, M.; Meerholz, K.; Braüchle, C.; Müllen, K. *Angew. Chem., Int. Ed.* **1998**, *37*, 1434–1437.
(18) Struijk, C. W.; Sieval, A. B.; Dakhorst, J. E. J.; van Dijk, M.; Kimkes, P.; Koehorst, R. B. M.; Donker, H.; Schaafsma, T. J.; Picken, S. J.; van de Craats, A. M.; Warman, J. M.; Zuilhof, H.; Sudhölter, E. J. R. *J. Am. Chem. Soc.* **2000**, *122*, 11057–11066.
(19) Würthner, F.; Thalacker, C.; Diele, S.; Tschierske, C. *Chem.—Eur. J.* **2001**, *7*, 2245–2253.
(20) Jancy, B.; Asha, S. K. *J. Phys. Chem. B* **2006**, *110*, 20937–20947.
(21) Li, X.Q.; Stepanenko, V.; Chen, Z.; Prins, P.; Siebbeles, L. D. A.; Wurthner, F. *Chem. Commun.* **2006**, 3871–3873.
(22) Sinks, L. E.; Rybtchinski, B.; Iimura, M.; Jones, B. A.; Goshe, A. J.; Zuo, X.; Tiede, D. M.; Li, X.; Wasielewski, M. R. *Chem. Mater.* **2005**, *17*, 6295–6303.
(23) Würthner, F. *Chem. Commun.* **2004**, 1564–1579.
(24) Sautther, A.; Thalacker, C.; Würthner, F. *Angew.Chem., Int. Ed.* **2001**, *40*, 4425–4428.
(25) Beckers, E. H. A.; Meskers, S. C. J.; Schenning, A. P. H. J.; Chen, Z.; Würthner, F.; Janssen, R. A. J. *J. Phys. Chem. A* **2004**, *108*, 6933–6937.
(26) Balakrishnan, K.; Datar, A.; Naddo, T.; Huang, J.; Oitker, R.; Yen, M.; Zhao, J.; Zang, L. *J. Am. Chem. Soc.* **2006**, *128*, 7390–7398.
(27) Datar, A.; Oitker, R.; Zang, L. *Chem. Commun.* **2006**, *1649*, 1651.

instrument was calibrated with indium standards before measurements. The phase behaviors of the molecules were analyzed using a hot stage polarized light microscope (Leitz-1350 heating stage coupled with PLM). WXRDs were recorded by a Philips analytical diffractometer using Cu Kα emission, and the spectra were recorded in the range of $2\theta = 2$–40° and analyzed using X'pert software. For SEM measurements, samples were provided with a thin gold coating using a JEOL JFC-1200 fine coater. The probing side was inserted into JEOL JSM- 5600 LV scanning electron microscope for taking photographs. A solvent-vapor annealing methodology was adopted for sample preparation. Thin films were fabricated by drop casting a $1 \times 10^{-5}$ M solution in toluene on to thin glass slides. These were subjected to solvent annealing by placing the films in a vacuum desiccator with a small vial of toluene inside. A slight vacuum was applied so as to saturate the desiccator with solvent vapor and the films were then left to anneal in the presence of the solvent for 12 h.

**Synthesis of 3,4,5-Tridodecyloxy Benzoyl Chloride (7).** 3,4,5-Trihydroxy benzoic acid (2 g, 2.96 mmol) was dissolved in a minimum amount of thionyl chloride (5 mL) and refluxed at 80 °C for 6 hours. The excess thionyl chloride was distilled off and washed three times with chloroform in order to remove all the thionyl chloride; the resultant acid chloride was used as such for further reactions. A similar procedure was used for the synthesis of 4-hydroxybenzoyl chloride. The synthesis of the intermediate *N,N′*-bis[6-hydroxyhexyl]perylene-3,4,9,10-tetracarboxyldiimide (**9**) is described in our earlier report.[20]

**Synthesis of Ester Functionalized Perylene Bisimides (1a, 2a, and 3a).** *N,N′-Bis[6-hexyl-3,4,5-tridodecyloxybenzester]perylene-3,4,9,10-tetracarboxyldiimide (**3a**).* A typical synthetic procedure is described for *N,N′*-bis[6-hexyl-3,4,5-tridodecyloxybenzester]-perylene-3,4,9,10-tetracarboxyldiimide (**3a**): *N,N′*-bis[6-hydroxyhexyl]perylene-3,4,9,10-tetracarboxyldiimide (**9**) (1 g, 1.6 mmol), in dry pyridine (15 mL), was heated to 80 °C under a nitrogen atmosphere; 3,4,5-tridodecyloxybenzoylchloride (3.52 g, 5.1 mmol) was added drop wise over a period of 15 minutes. The reaction mixture was stirred at 80 °C for 20 h. After being cooled to room temperature, it was poured into 50 mL of distilled water and extracted with chloroform. The solvent was then distilled off and the slurry washed several times with acetone to obtain a red powder. It was further purified by column chromatography using a chloroform/methanol (95:5 v/v) solvent mixture. Yield: 1.2 g (54%). $^1$H NMR (300 MHz, $CDCl_3$): $\delta$ 8.56–8.45 (dd, 8H, perylene), 7.05 (s, 4H, benzoyl), 4.23 (t, 4H, ester C**H**$_2$), 4.15 (t, 4H imide C**H**$_2$), 3.94 (t, 12H, OC**H**$_2$), 1.74–1.16 (m, 136H, C**H**$_2$), 0.816 (t, 18H, C**H**$_3$). $^{13}$C NMR ($CDCl_3$/TFA): $\delta$ 166.6, 162.7, 152.9, 142.4, 134.1, 131.1, 125.5, 122.9, 108.1, 73.6, 69.3, 65.2, 40.6, 32.1, 31.0, 30.5, 30.3, 29.9, 29.8, 29.7, 29.6, 29.5, 29.4. FTIR (KBr, cm$^{-1}$): 2922, 2851, 1693, 1662, 1594, 1497, 1462, 1430, 1344, 1223, 1121, 809, 747. Elemental anal. Calcd for $C_{122}H_{186}N_2O_{14}$: C, 76.93; H, 9.84; N, 1.47. Found: C, 76.34; H, 9.85; N, 1.43. MALDI-TOF MS (MW = 1904): $m/z = 1927.9$ $[M + Na]^+$.

*N,N′-Bis[6-hexyl-4-dodecyloxybenzester]perylene-3,4,9,10-tetracarboxyldiimide (**2a**).* Prepared from **9** (1 g, 1.6 mmol) and 4-dodecyloxy benzoyl chloride (1.66 g, 5.1 mmol). Purified by column chromatography using a chloroform/methanol (95:5 v/v) solvent mixture. Yield: 1.4 g (71%). $^1$H NMR (300 MHz, $CDCl_3$) $\delta$ ppm: 8.45–8.42 (dd, 8H, perylene), 8.03 (d, 4H, benzoyl), 6.93 (d, 4H, benzoyl), 4.29 (t, 4H, ester C**H**$_2$), 4.19 (t, 4H imide C**H**$_2$), 3.99 (t, 4H, OC**H**$_2$), 2.05–1.23 (m, 56H, C**H**$_2$), 0.895 (t, 6H, C**H**$_3$). $^{13}$C NMR ($CDCl_3$/TFA): $\delta$ 165.2,160.5, 135.6, 132.3, 129.4,126.4, 122.6, 69.1, 66.6, 32.2, 29.9, 29.8, 29.6, 29.5, 29.2. 28.5. 26.8. FTIR (KBr, cm$^{-1}$): 2919, 2846, 1711, 1695, 1656, 1593, 1510, 1469, 1254, 1165, 845, 808, and 743. Elemental anal. Calcd for $C_{74}H_{90}N_2O_{10}$: C, 76.13; H, 7.77; N, 2.40. Found: C, 75.89; H, 8.08; N, 2.37. MALDI-TOF MS (MW = 1166): $m/z = 1189.4$ $[M + Na]^+$.

**Synthesis of Amide Functionalized Perylene Bisimides (1b, 2b, and 3b).** *N,N′-Bis[6-hexyl-4-dodecyloxybenzamide]perylene-3,4,9,10-tetracarboxyldiimide (**2b**).* Prepared using PTCDA (0.88 g, 2.25 mmol), 4-dodecyloxy benzamide (1.90 g, 4.71 mmol), and zinc acetate (0.78 g, 4.93 mmol). Purified by silica gel column chromatography using a chloroform/methanol (95:5 v/v) solvent mixture. Yield: 350 mg (13%). $^1$H NMR (300 MHz, $CDCl_3$.TFA): $\delta$ 8.75 (s, 8H, perylene), 7.69 (d, 4H, benzoyl), 7.01 (d, 4H benzoyl), 4.27 (t, 4H, imide C**H**$_2$), 4.06 (t, 4H, OC**H**$_2$), 3.57 (t, 4H, amide C**H**$_2$), 3.45 (t, 4H, amideCH$_2$ C**H**$_2$), 1.27–1.82 (m, 52H C**H**$_2$), 0.861(s, 6H, C**H**$_3$). $^{13}$C NMR ($CDCl_3$, TFA): $\delta$ 165.3, 160.8, 135.7, 129.8, 126.4, 124.3, 122.3, 69.1, 42.2, 29.7, 29.5, 28.9, 28.2, 27.2, 25.7. FTIR (KBr, cm$^{-1}$): 3315, 3071, 2919, 2850, 1695, 1654, 1626, 1610, 1536, 1507, 1344, 1254, 809, 747. Elemental anal. Calcd for $C_{74}H_{92}N_4O_8$: C, 76.26; H, 7.96; N, 4.81. Found: C, 76.60; H, 7.44; N, 4.29. MALDI-TOF MS (MW = 1164): $m/z = 1165.8$ $[M + 1]^+$.

*N,N′-Bis[6-hexyl-3,4,5-tridodecyloxybenzamide]perylene-3,4,9,10-tetracarboxyldiimide (**3b**).* A typical synthetic procedure is described for *N,N′*-bis[6-hexyl-3,4,5-tridodecyloxybenzamide]perylene-3,4,9,10-tetracarboxyldiimide (**3b**): 3,4,5-tridodecyloxybenzoic acid (1 g, 1.5 mmol) was taken in a 50 mL round-bottomed flask under a nitrogen atmosphere, 5 mL of $SOCl_2$ was added, and the reaction mixture was stirred at 80 °C for 8 h. The excess $SOCl_2$ was distilled off under reduced pressure. Dry dichloromethane (DCM) ($3 \times 10$ mL) was added and rotovaped to remove the remaining traces of $SOCl_2$. This acid chloride was added slowly over a period of 30 min to an excess of hexamethylenediamine in 20 mL of dry DCM taken in a 100 mL two-neck round-bottomed flask. The reaction mixture was maintained under a $N_2$ atmosphere and cooled to 0 °C. The mixture was then gradually brought to room temperature and stirred for 12 h. For work up, the reaction mixture was washed with 1N HCl ($3 \times 50$ mL), extracted with $CHCl_3$, dried over anhydrous $CaSO_4$, and then evaporated to obtain amide **8** as a white solid. Perylene tetracarboxylic dianhydride (PTCDA) (2 g, 0.51 mmol), **8** (0.83 g, 11.2 mmol), and zinc acetate (0.20 g, 1.122 mmol) were mixed with 17 g of imidazole, and the reaction mixture was heated to 130 °C and kept there for 24 h. After being cooled to room temperature, 100 mL of methanol was added and the precipitate was collected and washed with additional methanol. After being dried in a vacuum, the crude product was purified by silica gel column chromatography using a chloroform/methanol (95:5 v/v) solvent mixture. Yield: 110 mg (12%). $^1$H NMR (300 MHz, $CDCl_3$.TFA): $\delta$ 8.78 (s, 8H, perylene), 6.91 (s, 4H, benzoyl), 4.27 (t, 4H, imide C**H**$_2$), 4.14 (t, 4H, OC**H**$_2$), 4.01 (8H, OC**H**$_2$), 3.51 (t, 4H, amide C**H**$_2$), 3.44 (t, 4H, amide CH$_2$ C**H**$_2$) 1.28–1.80 (m, 132 H C**H**$_2$), 0.863(s, 18H, C**H**$_3$). $^{13}$C NMR ($CDCl_3$, TFA): $\delta$ 166.3, 161.3, 136.5, 133.6, 129.9, 126.9, 126.8, 71.4, 32.4, 30.4, 30.2, 30.1, 29.9, 29.8. FTIR (KBr, cm$^{-1}$): 3269, 3093, 2917, 2851, 1674, 1654, 1626, 1591, 1577, 1503, 1465, 1341, 1240, 1111, 817. Elemental anal. Calcd for $C_{122}H_{188}N_4O_{12}$: C, 77.01; H, 9.96; N, 2.94. Found: C, 77.43; H, 8.78; N, 2.74. MALDI-TOF MS (MW = 1900): $m/z = 1900.3$ $[M]^+$.

The syntheses of compounds **1a**, **2a**, **4**, **5**, and **9** were reported earlier.[20]

## Results and Discussion

The structures of the perylenebisimide esters and amides are shown in Scheme 1. The typical synthetic procedure for ester series and amide series is demonstrated with examples for per6tridodecbenzester (**3a**) and per6tridodecbenzamide

**Scheme 1. Structure of Perylenebisimide Ester and Amide Molecules**

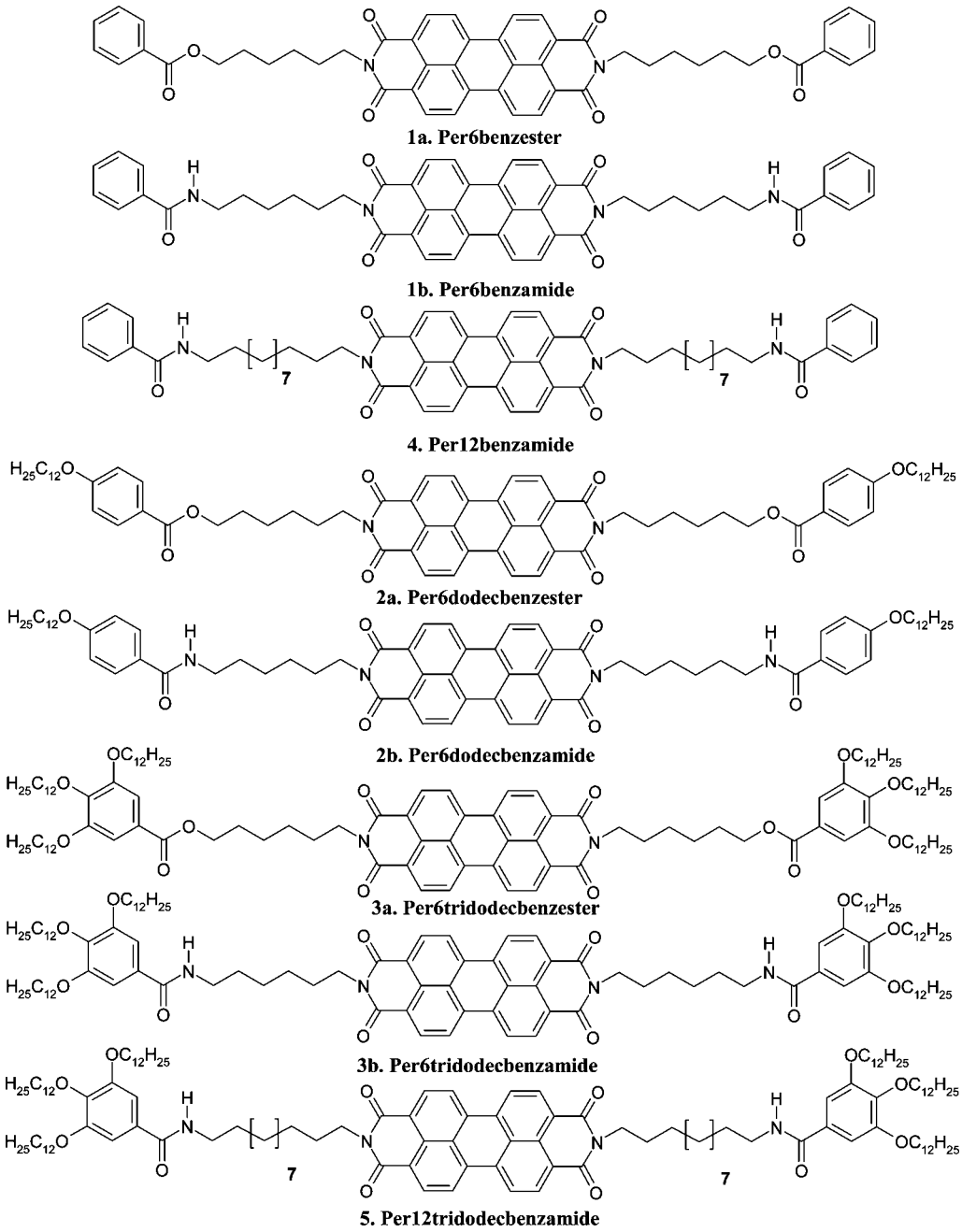


(**3b**), respectively, in Scheme 2. A core-to-periphery approach was adopted for synthesis of ester series, whereas a periphery-to-core approach was adopted in the case of amide series.[28] For the synthesis of the ester molecule, perylene tetracarboxylic dianhydride (PTCDA) was first coupled with ~2.2 equiv. of 6-amino hexanol to obtain the hydroxyl terminated unit **9**. 3,4,5-Tridodecyloxy benzoyl chloride (**7**) was synthesized adopting literature procedure.[21,29] Two equivalents of this acid chloride was coupled with **9** to obtain the ester-functionalized perylenebisimide hexyl spacer and tridodecyloxy benzyl termini (**3a**). For the synthesis of the amide molecule with similar spacer and end termini, the acid chloride **7** was coupled with an excess of 1,6-diamino hexane to obtain the amine-terminated unit **8**. Two equivalents of **8** were coupled with PTCDA to obtain perylenebisimide hexyl spacer having tridodecyloxy benzyl termini (**3b**) with amide functionality. The other members of the ester and amide series were synthesized similarly using appropriate acid chlorides. For instance, benzoyl chloride was used for the synthesis of **1a**, **1b**, and **4**; 4-dodecyloxy benzoyl chloride was used for the synthesis of **2a** and **2b**; and 3,4,5-tridodecyloxy benzoyl chloride was used in the synthesis of **3a**, **3b**, and **5**. The longer spacer amides (**4** and **5**) having dodecyl spacer segments between perylene core and termini

(28) Schenning, A. P. H. J.; Meijer, E. W. *Chem. Commun.* **2005**, *3245*, 3258.

(29) Hersmis, M. C.; Spiering, A. J. H.; Waterval, R. J. M.; Meuldijk, J.; Vekemans, J. A. J. M.; Hulshof, L. A. *Org. Process Res. Dev.* **2001**, *5*, 54–60.

(30) In our previous report, a core-to-periphery approach was adopted for the synthesis of amides; however, the periphery-to-core route adopted in the current report seemed to provide an easier route compared to the former.

**Scheme 2. Synthesis of the Benzoyl Ester and Amide Series**

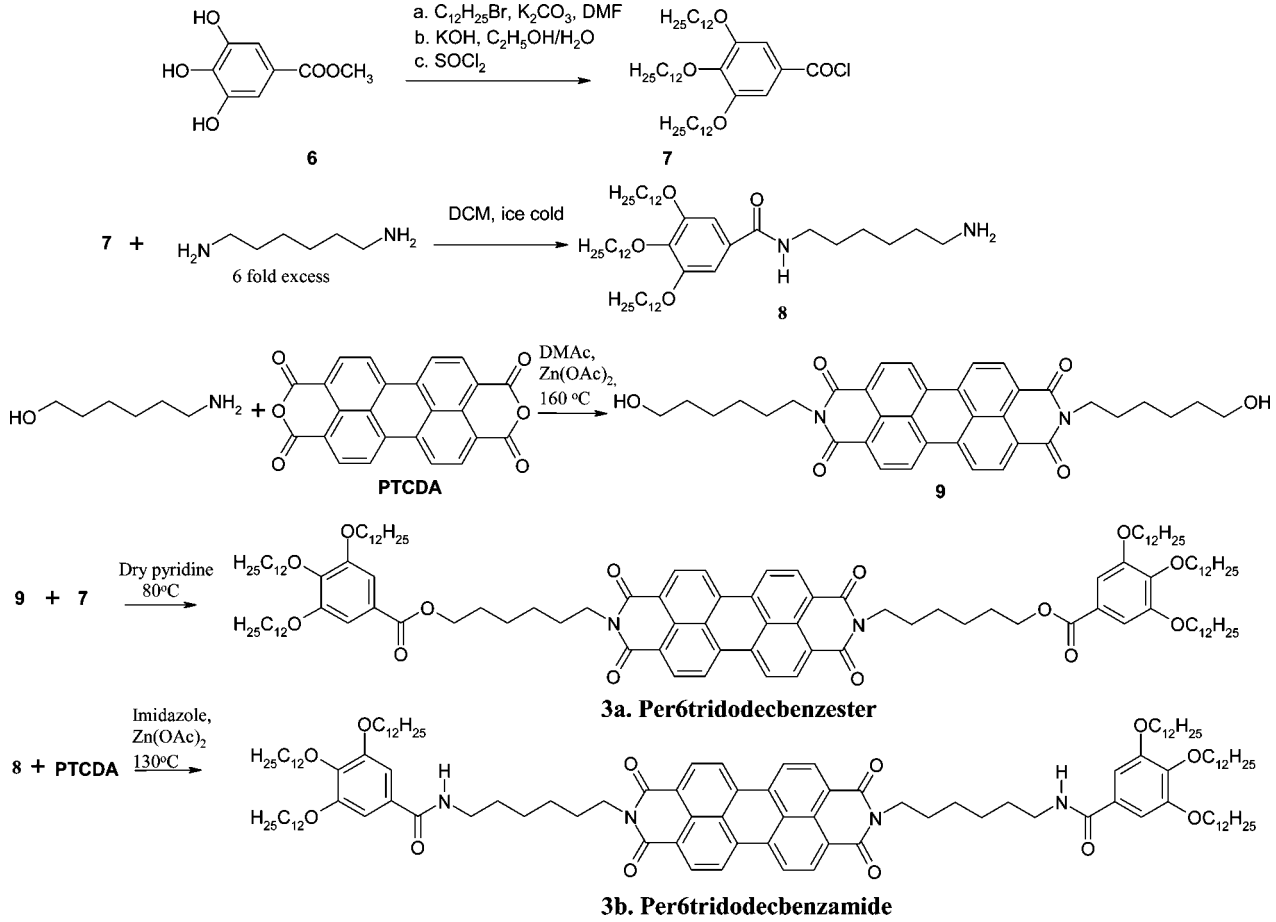


were synthesized as reported earlier.[30] All the compounds were fully characterized by $^1H$ and $^{13}C$ NMR spectroscopy, size exclusion chromatography (SEC), and MALDI-TOF mass spectroscopy after being subjected to meticulous purification procedures by repeated column chromatography. The SEC analysis (see the Supporting Information, Figure S1) showed single peaks for all the compounds confirming their purity. As expected, the compounds having higher mass eluted earlier compared to those with lower mass. Also, the amide and ester molecules of each series differed in mass by only 2 units, which is reflected well in the SEC data. The MALDI-TOF mass spectra were recorded using 2,5-dihydroxy benzoic acid as the matrix and molecular ion peaks were obtained for either $[M + 1]^+$ or cationic species such as $MNa^+$, $MK^+$, and $MZn^+$. The sodium and potassium ions are from solvents and the $Zn^+$ ions were picked from trace amounts (parts per million level) of the $Zn(OAc)_2$ catalyst left after purification.[20] For example, the mass spectrum of per6dodecbenzamide (**2b**) showed peaks corresponding to $M^+$ peak at 1164.8 and peak corresponding to $MZn^+$ ion minus the dodecyl unit at 1063.0 (see the Supporting Information, Figure S2). The single peak in the SEC coupled with the mass spectra from MALDI-TOF reaffirmed the high purity of the molecules under study. The structure of the molecules was confirmed by proton NMR spectra. Figure 1 shows the proton NMR spectra of the per6tridodecbenzester (**3a**) and per6tridodecbenzamide (**3b**) with the peaks labeled. The intensities for the 8 aromatic protons of the perylene ring (labeled a) was double that of the four aromatic protons of the tridodecyloxy benzene unit (labeled b) in both cases, confirming the formation of the molecules. The splitting of the aromatic protons of perylene into two doublets is observed only when $CDCl_3$ alone is used as the NMR solvent and is not observed when trifluoroacetic acid (TFA) is also added for solubility reasons.[20] One interesting feature that is immediately apparent on comparing the spectra of the amide and ester series is the change in the splitting pattern of peaks in the 3.5−4.5 ppm region. In all the amide spectra,

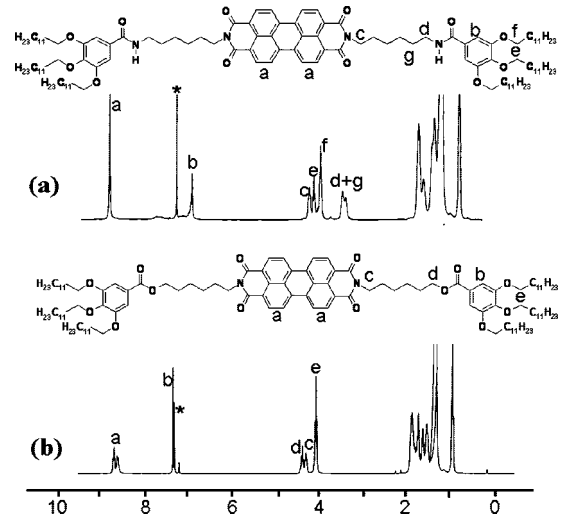


**Figure 1.** $^1H$ NMR spectra of (a) per6tridodecbenzamide and (b) per6tridodecbenzester. Spectrum a is recorded in $CDCl_3/CF_3COOH$ and b is recorded in $CDCl_3$

regardless of the presence or absence of substitution on the terminal benzene ring, additional peaks were observed at ~3.5 ppm. In the ester series, only three peaks corresponding to the four $CH_2$ protons next to the ester (labeled d), four $CH_2$ protons next to the perylene imide (labeled c), and protons corresponding to the $OCH_2$ of the alkoxy substitution on the terminal benzene ring (labeled e) are present in the 3.8−4.5 ppm region. In the corresponding amide series, the four $CH_2$ protons next to the perylene imide (labeled c) appears upfield compared to the four $CH_2$ protons next to the terminal amide (labeled d). Additionally, four inner $CH_2$ protons next to the terminal amide (labeled g) appear in the 3.45 ppm range in all three amide series. In the case of per6tridodecbenzamide (**3b**), a total of five peaks appear in the 3.5−4.5 ppm region. The $OCH_2$ protons corresponding to the alkoxy substitution is once again split as four protons corresponding to the para $OCH_2$ (labeled e) and eight protons corresponding to the meta positions (labeled f). This electronic effect is present even when the spectra are recorded in the presence of TFA, indicating that it is not due to aggregation effect, which would have been disrupted in the presence of acid.

**Optical Properties.** The optical properties of the perylenebisimide amide and ester series were investigated by UV/vis and fluorescence spectroscopy in solvents like dichloromethane (DCM), tetrahydrofuran (THF) and toluene (see the Supporting Information, Figure S7). Maximum aggregation tendency was observed in toluene. The absorption spectra of a $1 \times 10^{-6}$ M solution of the amide series and ester series in toluene are given in panels a and b in Figure 2, respectively, and their optical data are summarized in Table 1. Three important aspects became immediately apparent from the figure: (1) the amide and ester series showed different modes of aggregation behavior; (2) all the molecules in the amide series were highly aggregated, whereas only the per6dodecbenzester (**2a**) showed aggregation behavior in the ester series; and (3) in both series, it was the mono alkylated benzene substitution that showed maximum aggregation tendency. The absorption spectra of perylene tetracarboxylic diimides normally show four peaks in the range of 450–525 nm, which corresponds to 0–0, 0–1, 0–2, and 0–3 electronic transitions, respectively. It can be seen from the figure that in the amide series, the transition from the ground level to the higher levels of electronic state (0–1, 0–2, and 0–3) was enhanced compared to 0–0 transition.[26] Additionally, a predominant peak corresponding to aggregation was also found at a higher wavelength centered at 570 nm. On the other hand, in the ester series, a small peak corresponding to aggregation was found centered at 570 nm for the per6dodecbenzester (**2a**) and the 0–0, 0–1, 0–2, etc., vibronic transitions showed the characteristic behavior of a perylenebisimide molecule. A variable concentration ($3 \times 10^{-5}$ to $1 \times 10^{-6}$ M) UV−vis absorption measurements were carried out in toluene for both the amide and ester series and are given in Figure 3. As can be seen from the figure, a slight increase in the intensity of the aggregation peak was observed for per6dodecbenzester (**2a**), whereas per6benzester (**1a**) and per6tridodecbenzester (**3a**) continued to remain in the molecularly dissolved form even in the highest concentrated solution.

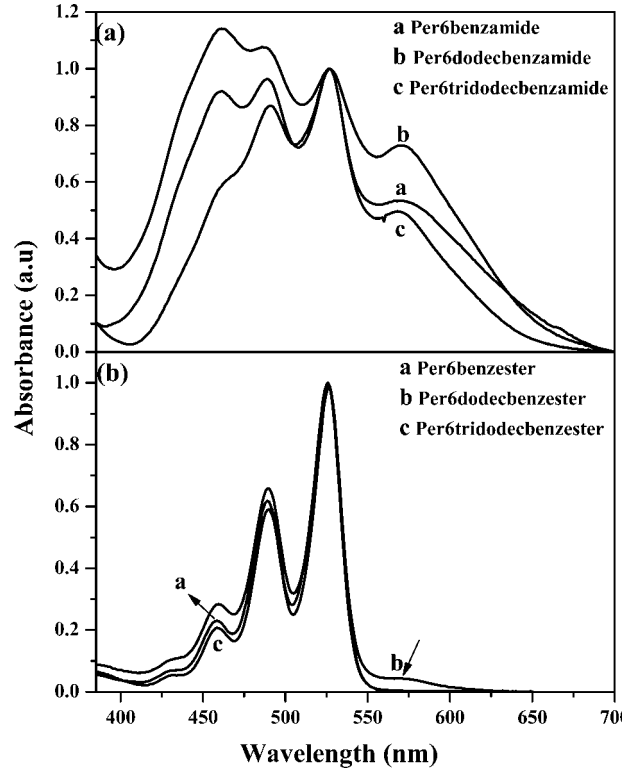


**Figure 2.** Normalized absorption spectra of the (a) perylene amide series and (b) perylene ester series in toluene.

The presence of the new peak (albeit small in intensity) at 570 nm is indicative of aggregation. The aggregation was further supported by temperature dependence of the absorption spectra. The intensity of the aggregated peak at 570 nm for the per 6 dodecbenzester (**2a**) increased upon the temperature being lowered to 10 °C, and the absorption band also red shifted compared to that at high temperature (shown in the Supporting Information, Figure S8). The disappearance of the aggregation peak at 90 °C pointed to the dissolution of the aggregates at high temperature. This behavior indicated J type aggregate formation at low temperatures or high concentration, similar to that reported in literature.[31] However, pronounced spectral changes like broadening of the spectra and loss of vibronic fine structures, were observed upon increasing the concentration of the amide series. As the concentration was increased in the amide series, the ratio of the intensities of the 0–0/0–1 decreased, and at very high concentration, the 0–1 peak became more intense compared to the 0–0 peak.[32] This difference in intensity on going from dilute to concentrated solution can be considered as being due to the presence of an additional blue-shifted band at around 450 nm.[18] The intensity of the aggregated peak at 570 nm also increased with an increase in concentration. The existence of both blue- and red-shifted bands in the absorption spectra has been explained on the basis of the Kasha's model for point dipole.[33,34] According to the model, the red or blue shift of the absorption band is based on the angle

(31) Beckers, E. H. A.; Chen, Z.; Meskers, S. C. J.; Jonkheijm, P.; Schenning, A. P. H. J.; Li, Xue-Quing.; Osswald, P.; Würthner, F.; Janssen, R. A. J. *J. Phys. Chem. B* **2006**, *110*, 16967–16978.
(32) Gomez, R.; Veldman, D.; Blanco, R.; Seoane, C.; Segura, J. L.; Janssen, R. A. J. *Macromolecules* **2007**, *40*, 2760–2772.

**Table 1. Spectroscopic Data**

| | solution (in toluene) | | | | film (on glass plate) | | |
|---|---|---|---|---|---|---|---|
| compd | $\lambda_{max}$[a] (abs) | $\epsilon$ (L mol$^{-1}$ cm$^{-1}$) | $\lambda_{max}$[c] (em) | $\varphi_{FL}$[d] | $\lambda_{max}$[b] (abs) | $\lambda_{max}$[c] (em) | PL intensity ($1 \times 10^5$)[c] (UV absorbance value) |
| per6benzester (**1a**) | 525 | $4.93 \times 10^4$ | 547 | 0.81 | 496 | 675 | 30 (0.16) |
| per6dodecbenzester (**2a**) | 525 | $7.14 \times 10^4$ | 546 | 0.80 | 495 | 672 | 64 (0.17) |
| per6tridodecbenzester (**3a**) | 525 | $6.84 \times 10^4$ | 544 | 0.81 | 493 | 672 | 86 (0.15) |
| per6benzamide (**1b**) | 525 | $2.40 \times 10^3$ | 545 | 0.65 | 504 | 677 | 63 (0.05) |
| per6dodecbenzamide (**2b**) | 525 | $6.56 \times 10^3$ | 546 | 0.50 | 491 | 669 | 56 (0.33) |
| per6tridodecbenzamide (**3b**) | 525 | $1.33 \times 10^4$ | 544 | 0.60 | 493 | 674 | 2.0 (0.13) |

[a] Values correspond to the 0–0 transition. [b] Values correspond to transition from ground to higher electronic level (0–1). [c] Excitation energy is corresponding absorption maxima. [d] The fluorescence quantum yields were obtained upon excitation at 524 nm and were measured using rhodamine-6G as a standard.

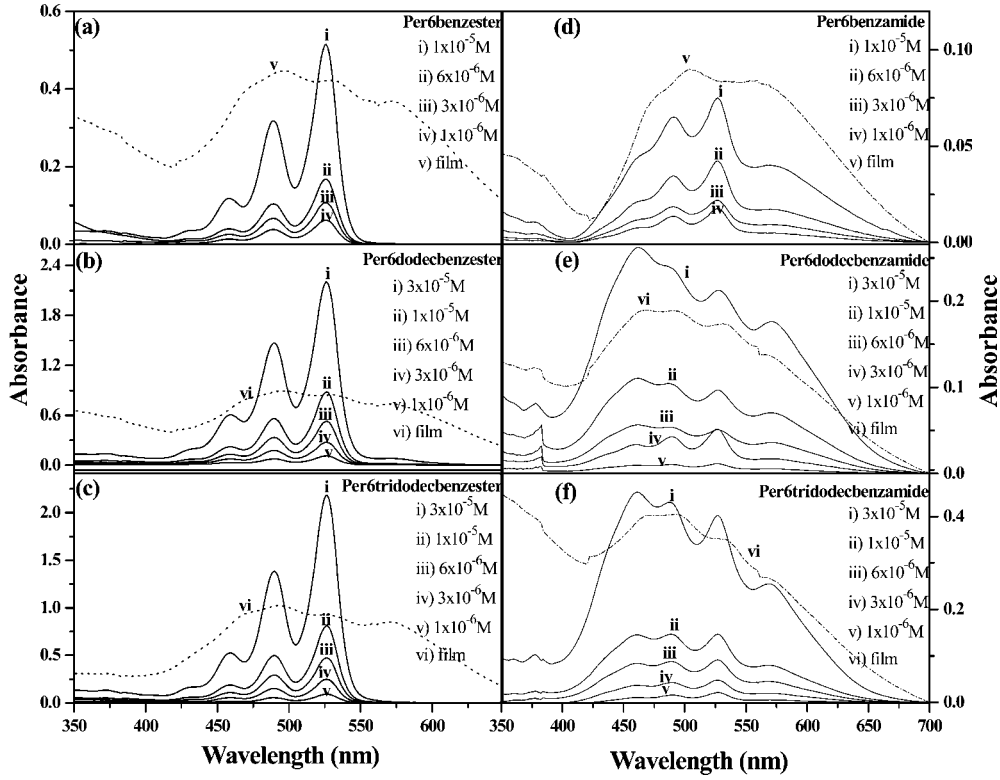


**Figure 3.** Concentration-dependent UV−vis measurements of (a) per6benzester **1a**, (b) per6doodecbenzester **2a**, (c) per6tridodecbenzester **3a**, (d) per6benzamide **1b**, (e) per6dodecbenzamide **2b**, and (f) per6tridodecbenzamide **3b** in toluene at room temperature. Dotted line indicates the UV−vis spectrum of drop-cast films.

between the center-to-center vector and the transition dipole moments of the molecule. If the transition dipole moments are not parallel but slightly rotated with respect to each other, both blue- and red-shifted bands are seen in the absorption spectra of the molecule.[18,35] On the basis of these characteristic features in the absorption spectra recorded in toluene for the amide and ester series of the perylenebisimides, the aggregation behavior can be identified as being due to the formation of cofacial H type aggregates in the amide series and displaced core J type aggregates in the ester series, respectively.

The UV−vis absorption spectra of drop-cast films of the sample from toluene solution are also shown as a dotted line in Figure 3. The film absorption matched the solution spectra very well in the amide series, indicating the high level of aggregation already present in solution in this series. In the case of the ester series, the absorption spectra of the films showed the emergence of a new peak at ~570 nm and they resembled the thin-film spectra of the amide series, indicating that in the solid state, the ester series exhibited H type aggregate formation like the perylenebisimide amide molecules.

The emission spectra of the perylenebisimide amide and ester series were recorded in toluene at a concentration of $1 \times 10^{-6}$ M and are given in Figure 4a. The fluorescence spectra showed the characteristic features of perylenebisimides reported in the literature and they have a mirror image relationship with the absorption. In general, for the H type of aggregates, a fluorescence quenching is expected. However, the fluorescence of the amide series was not quenched, although the quantum values were very much reduced compared to that of the ester series. The quantum yield values

(33) McRae, E. G.; Kasha, M. J. *Chem. Phys.* **1958**, *28*, 721.
(34) Kasha, M. In *Spectroscopy of the Excited State*; Di Bartolo, B., Ed.; Plenum Press: New York, 1976; pp 337–363.
(35) Chen, Z.; Baumeister, U.; Tschierske, C.; Würthner, F. *Chem.−Eur. J.* **2007**, *13*, 450–465.

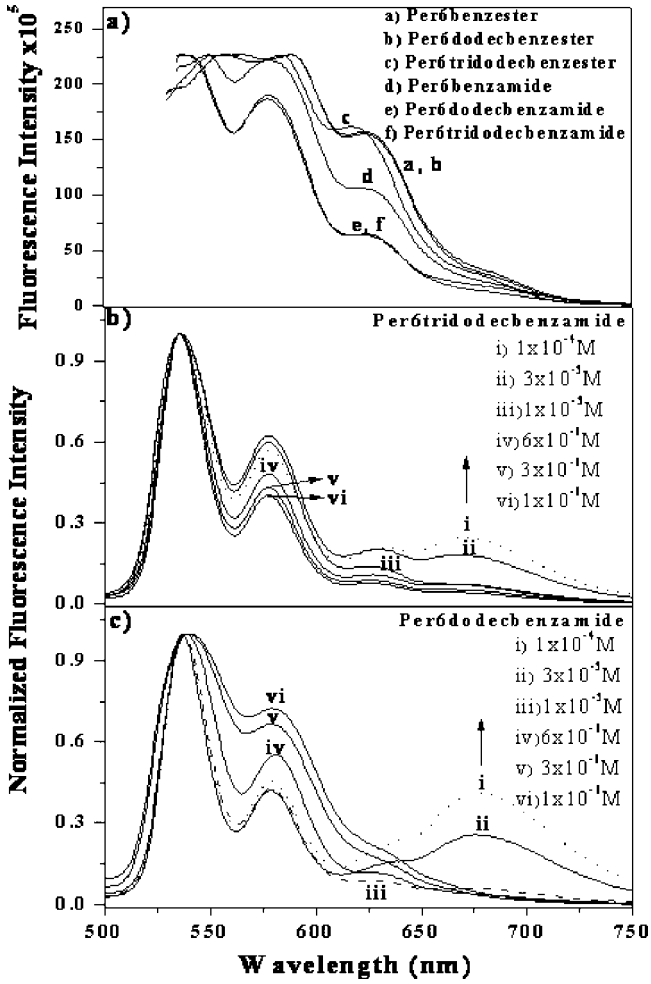


**Figure 4.** Fluorescence spectra of (a) perylenebisimide derivatives recorded in toluene at a concentration of $1 \times 10^{-6}$ M and concentration-dependent fluorescence spectra normalized at 536 nm (excited at $\lambda_{ex} = 461$ nm) of (b) per6dodecbenzamide and (c) per6tridodecbenzamide in toluene. The arrows indicate the changes upon increasing the concentration.

of the amides was ~0.5–0.65 compared to 0.8 for the esters. The quantum yields were calculated for all samples in toluene using rhodamine-6G as standard in water and are given in Table 1. A concentration-dependent fluorescence measurement ($1 \times 10^{-4}$ to $1 \times 10^{-6}$ M) was carried out for per 6 dodecbenzamide (**2b**) and per6tridodecbenzamide (**3b**) in toluene. Their fluorescence spectra normalized at 536 nm are shown in panels c and b, respectively, of Figure 4, with the arrow indicating the direction of change upon increasing the concentration. Both spectra display the emergence of a new emission band centered at 670 nm at higher concentration, which corresponds to the emission from the aggregates. The intensity of this new aggregation band increases with increasing concentration, with its long tail region reaching the near infrared (NIR).[36,37] However, such an observation was not found in the case of per6dodecbenzester (**2a**) upon increasing the concentration. The photoluminescence spectra were recorded for thin drop-cast films of the samples from

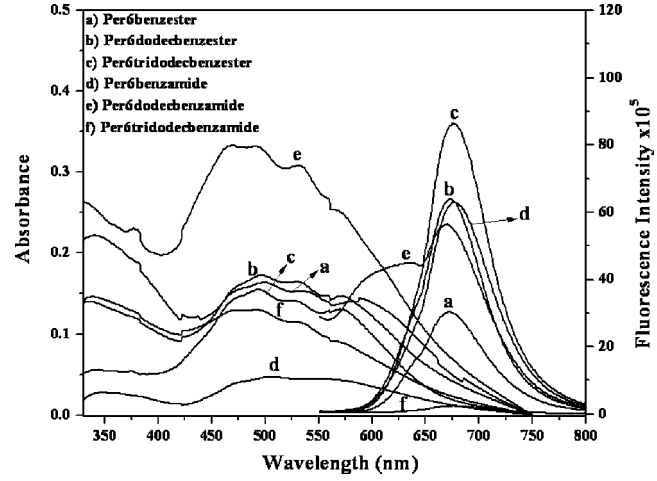


**Figure 5.** UV−vis and emission spectra of drop-cast films from toluene.

toluene solution. Figure 5 shows the combined absorbance and photoluminescence spectra of the samples. For each sample, films of different thickness were prepared by drop-casting from solutions of different concentrations and films having optical density in the range ~0.1 at their $\lambda_{max}$ values were chosen for the photoluminescence measurements. The PL spectra were obtained by exciting at the $\lambda_{max}$ values, and for each sample, the spectra were recorded at different locations to confirm the uniformity of film thickness. The $\lambda_{max}$ values for the UV absorbance and PL intensity for the thin films are reported along with their optical density in Table 1. It can be seen from Figure 5 and Table 1 that per6tridodecbenzamide (**3b**) showed quenching of fluorescence, as expected from an H type aggregate. However, the other two amide series molecules did not show a quenching of fluorescence. The emission $\lambda_{max}$ values for the films were all red-shifted and centered at 670 nm compared to that of the corresponding solution spectra, indicating strong $\pi-\pi$ stacking. Similar behavior was observed by Würthner et. al for a tridodecylphenyl-substituted perylene derivative that showed typical H type aggregation behavior in its absorption and emission spectrum.[36] The concentration-dependent fluorescence spectra of the sample showed the formation of a new broad aggregate emission band at 600–850 nm, which matched perfectly with the emission from spin-coated thin film. The origin of this emission even for H type aggregates was rationalized on the basis of molecular exciton theory by assuming rotational displacements in the $\pi-\pi$ stacking with displacement angles of 70–80°.[36,37] A similar argument in our example is also in accordance with the conclusion of slightly rotated transition dipoles based on the existence of both a blue- and red-shifted band in the UV−vis spectra.

Temperature-dependent UV−vis analysis was carried out for all the molecules in toluene from 80 to 20 °C and the behavior of the amide series at a concentration of $3 \times 10^{-6}$ M is given in Figure 6. The arrows indicate the direction of change upon increasing the temperature and the spectra are normalized with respect to the one at the highest temperature. The dotted line indicates the same spectra at room temperature upon addition of a drop of TFA. Addition of TFA completely removes the aggregation and also solubilizes the molecules better resulting in a hyperchromic shift of the peak.

(36) Würthner, F.; Chen, Z.; Dehm, V.; Stepanenko, V. *Chem. Commun.* **2006**, 1188–1190.
(37) Chen, Z.; Stepanenko, V.; Dehm, V.; Prins, P.; Siebbeles, L. D. A.; Seibt, J.; Marquetand, P.; Engel, V.; Würthner, F. *Chem.—Eur. J.* **2007**, *13*, 436–449.

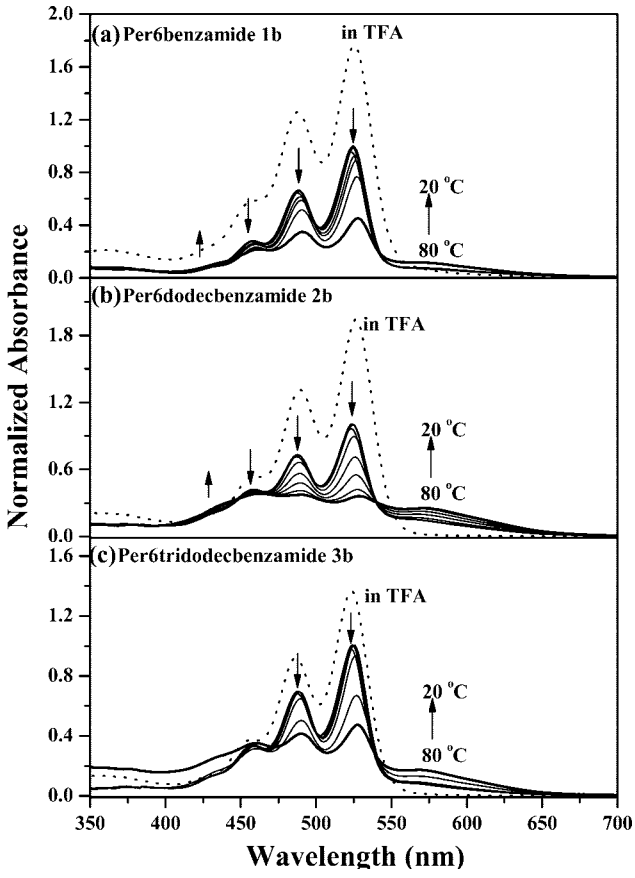


**Figure 6.** Temperature-dependent UV−vis measurements of $3 \times 10^{-6}$ M solution of (a) per6benzamide **1b**, (b) per6dodecbenzamide **2b**, and (c) per6tridodecbenzamide **3b** in toluene.

The transition from the molecularly dissolved state to the aggregated form as a function of temperature is plotted for all the molecules (ester and amide series) in Figure 7. The absorbance values of the aggregated species (~570 nm) are taken from the normalized spectra as depicted in figure 6. Therefore, a direct comparison of the absolute values of the absorbance of the aggregated molecules among the series can be taken to depict the strength of their aggregation. Per6dodecbenzamide (**2b**) has the highest extent of aggregation among the four aggregated molecules, and the transformation from the aggregated to the molecularly dissolved species as indicated by the change of slope occurs around 60 °C. In per6tridodecbenzamide (**3b**) and per6dodecbenzester (**2a**), this transition occurs at ~50 °C, whereas in per6benzamide (**1b**), the transition happens much earlier, at ~40 °C. Among the four molecules, the per6dodecbenzester (**2a**) showed the least extent of aggregation, which is also indicated by the low intensity of the aggregation peak at 570 nm. The striking difference in the behavior of the amide versus ester is evident in the example of **2a** and **2b**. The amide **2b** showed the highest extent of aggregation, whereas the analogous ester **2a** showed the least aggregation tendency, although it was the highest among the ester series. The aggregation in the ester molecule is due to the $\pi-\pi$ interaction of the perylenebisimide aromatic core, whereas this interaction is further strengthened by the hydrogen bonding in the amide series. Another interesting feature of the structure−property relationship is highlighted by the comparison between the monododecyloxy and tridodecyloxy

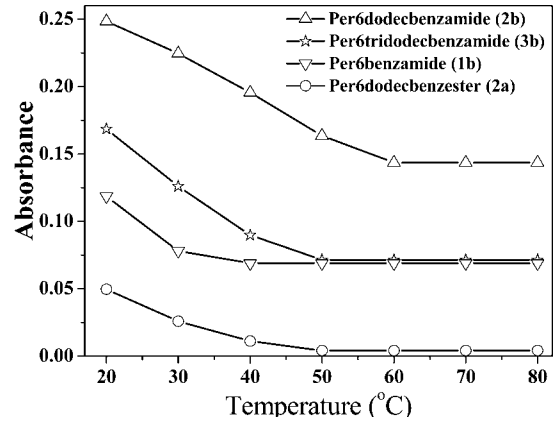


**Figure 7.** Plot of the absorbance of the aggregates vs temperature at the concentration of $3 \times 10^{-6}$ M.

substitution of the terminal benzene ring. Whereas the monododecyloxy substitution supported aggregate formation as illustrated in both amide and ester series by the higher extent of aggregate formation in per6dodecbenzamide (**2b**) in the amide series and per6dodecbenzester (**2a**) in the ester series, the tridodecyloxy substitution disrupted the $\pi-\pi$ interaction. This is evident from the complete absence of any aggregation in per6tridodecbenzester (**3a**) even at very high concentrations (see Figure 3c). That the long terminal alkyl chain has a decisive role to play in stabilizing the aggregates is illustrated by the lowest extent of aggregation and lowest transition temperature (~40 °C) in the unsubstituted terminal benzene system, per6benzamide (**1b**). This was quite surprising because one would have expected higher self-organization in **1b** because of a lack of steric hindrance when compared to its substituted counter parts. Similarly, in the ester series, contrary to the expectation of a better $\pi-\pi$ interaction in the unsubstituted system, per6benzester (**1a**), the trend of the monododecyloxy substitution having the highest aggregation tendency was reflected in the ester series as well, with only per6dodecbenzester 2a showing aggregation behavior in toluene. Thus the optimum balance of structural parameters like rigidity and flexibility and steric hindrance is reached in the monododecyloxy-substituted system, resulting in it exhibiting the highest level of self-organization as compared to the unsubstituted or tridodecyloxy-substituted terminal benzene ring in both the amide and ester series. Figure 8 shows the schematic representation of the proposed J type packing in solution in per6dodecbenzester **2a** and the rotationally displaced H type of packing that is present in solution as well as in the solid state in per6dodecbenzamide **2b**.

**Liquid-Crystalline Properties.** The phase behavior of the samples was investigated with differential scanning calorimetry (DSC), polarized light microscopy (PLM), and X-ray diffraction measurements. The thermal stability of the perylenebisimide molecules were studied by thermogravimetric analysis (TGA) under nitrogen atmosphere and the 10 wt % loss temperatures are given in Table 2. The ester series had a higher 10 wt % loss temperature compared to the corresponding amide molecules. The second heating and first cooling thermograms in the DSC of the perylenebisimide molecules are shown in Figure

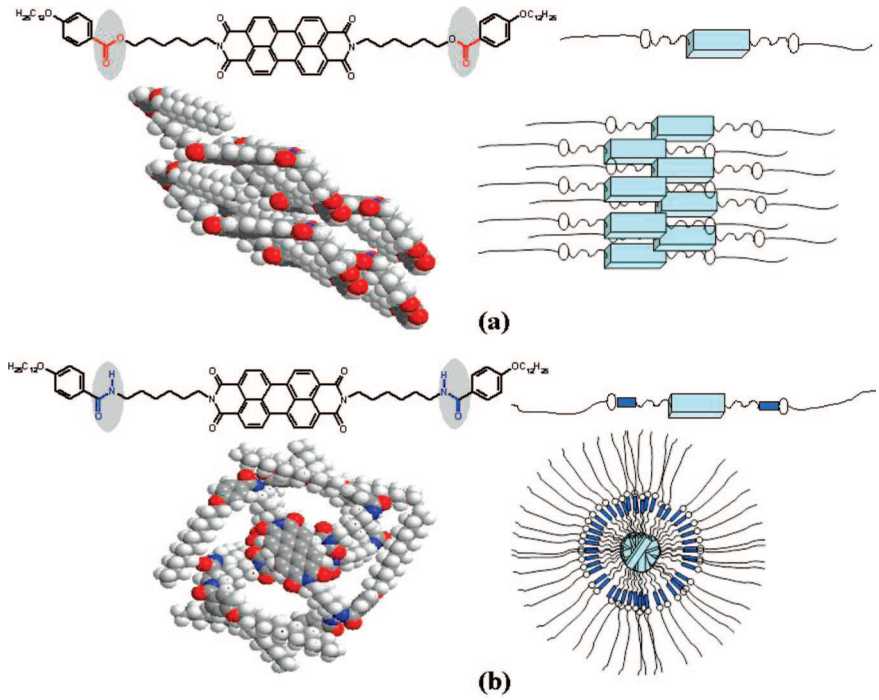


**Figure 8.** Schematic diagram of the packing in (a) J type aggregates of per6dodecbenzester **2a** in solution and (b) H type aggregates of per6dodecbenzamide **2b** in solution as well as solid state.

**Table 2. Thermal Data**

| compd | $T_m$[a](C−LC) (°C) | $\Delta H_m$[a](C−LC) (J/g) | $T_m$[a](LC−I) (°C) | $\Delta H$[a](LC−I) (J/g) | $T_c$[b](I−LC) (°C) | $\Delta H_c$[b](I− LC) (J/g) | $T_c$[b](LC−C) (°C) | $\Delta H_c$[b](LC−C) (J/g) | $T_D$[c] (°C) |
|---|---|---|---|---|---|---|---|---|---|
| per6benzester (**1a**)[d] | 239.4 | 64.43 | 257.2 | 1.14 | 222.7 | 10.12 | 180.4 | 46.25 | 314 |
| per6benzamide (**1b**)[d] | | | 216.3 | 6.16 | 189.1 | 3.92 | | | 276 |
| per12benzamide (**4**)[d] | 164.7 | 3.34 | 206.0 | 9.50 | 192.9 | 5.36 | | | 262 |
| per6dodecbenzester (**2a**) | 73.8 | 0.52 | 229.0 | 35.5 | 219.1 | 32.5 | 58.7 | 1.49 | 383 |
| per6dodecbenzamide (**2b**) | 146.2 | 21.0 | 249.0 | 16.12 | 231.7 | 13.17 | 129.1 | 18.4 | 295 |
| per6tridodecbenzester (**3a**) | | | 137.0 | 39.1 | 107.9 | 41.4 | | | 388 |
| per6tridodecbenzamide (**3b**) | 36.9 | 3.90 | 131.5 | 16.8 | 113.3 | 8.67 | 25.64 | 3.89 | 372 |
| per12tridodecbenzamide (**5**)[d] | 91.5 | 0.94 | 172.7 | 22.48 | 144.7 | 1.37 | 82.7 | 0.34 | 396 |

[a] Measured for the quenched sample in the second heating cycle at 10 °C/min heating rate. [b] Measured for the first cooling cycle from the melt at 10 °C/min cooling rate. [c] Temperature represents 10% weight loss in TGA measurements at heating rate of 10 °C/min under nitrogen. [d] Data from earlier report.

9. Table 2 summarizes the phase-transition temperatures and corresponding enthalpy changes $\Delta H$. All molecules except per6benzamide (**1b**) showed multiple transitions in the DSC thermogram. Per6benzester (**1a**) showed a transition from the pristine state to the LC phase at 239.4 °C with $\Delta H$ value of 64.43 J/g. This large value of $\Delta H$ indicates a high crystallinity of the pristine state, which was confirmed by the X-ray diffraction measurements at room temperature. The per6dodecbenzester (**2a**) had the largest liquid crystal window among the whole series −170 °C. The crystal to LC transition occurred with a very weak enthalpy change of ∼75 °C followed by a melting to isotropic phase at ∼229 °C with a large enthalpy value of $\Delta H = 35.5$ J/g. Similarly, in its cooling cycle, the isotropic to LC transition occurred with large enthalpy of $\Delta H = 32.5$ J/g followed by a couple of weak transitions at ∼60 °C. PLM photographs of some of the liquid-crystalline molecules are given in Figure 10. These were all taken during the cooling scans as the sample solidified from the isotropic melt into liquid crystalline phases. Images a and b in Figure 10 are the texture obtained for per6dodecbenzester (**2a**) upon cooling to 202 and 64 °C, respectively. Initially, the sample formed large platelike structures that, upon further cooling beyond 70 °C, converged to form densely packed threaded textures. Per6tridodecbenzester (**3a**) had only a very narrow liquid-crystal window in the heating cycle (∼4 °C), as seen from the small shoulder at 134 °C along with the main transition at 137 °C. Upon cooling, only one sharp transition was observed at 108 °C with $\Delta H = 41.4$ J/g, which indicates a supercooling usually observed for columnar mesophases.[35] PLM observation showed a texture only during the cooling cycle from the isotropic melt; however, the sample remained frozen in the liquid-crystalline phase upon cooling to room temperature. Figure 10c shows the features formed at 98 °C upon cooling in the case of **3a**.

In the amide series, amide **1b** was not liquid crystalline and showed only clear melting and crystallization peak in the heating and cooling cycles, respectively. Per6dodecbenzamide (**2b**) had a liquid-crystal window of 103 °C (the largest in this series) and showed two transitions at 146 and 249 °C with enthalpy values $\Delta H = 21$ and 16 J/g, respectively. Per6tridodecbenzamide (**3b**) had an LC window

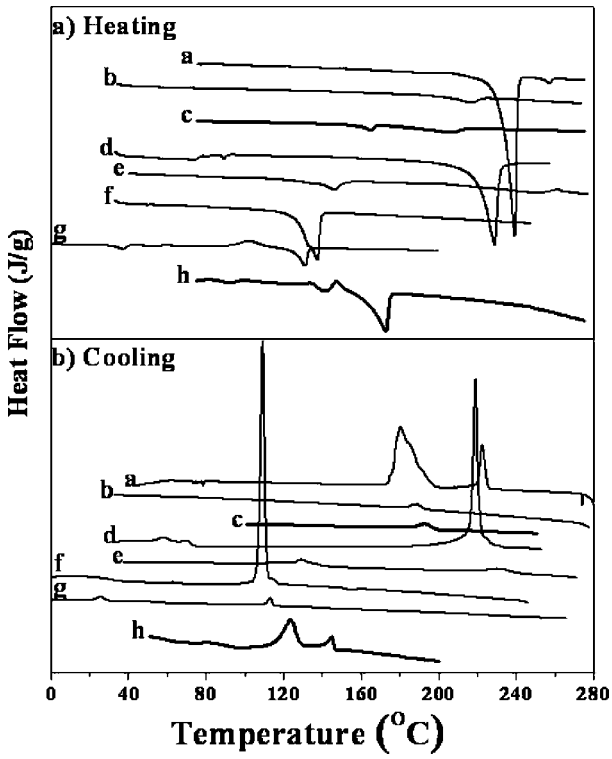


**Figure 9.** Differential scanning calorimetry (DSC) thermograms of the second heating scans and first cooling scans of perylene-based amides (spacer 12 dark straight line) and esters. The samples are (a) per6benzester, (b) per6benzamide, (c) per12benzamide, (d) per6dodecbenzester, (e) per6dodecbenzamide, (f) per6tridodecbenzester, (g) per6tridodecbenzamide, and (h) per12tridodecbenzamide.

of 95 °C and exhibited multiple transitions with exothermic transition corresponding to recrystallization in the heating cycle. The LC textures of **2b** and **3b** are shown in Figure 10 d−f. The liquid-crystal textures for samples **1a**, **4**, and **5** have been discussed in our earlier report.[20]

Comparison across the ester and amide series was accomplished by classifying the molecules into three groups: (a) molecules lacking a terminal substitution, (b) molecules with monododecyloxy terminal substitution, and (c) molecules with tridodecyloxy terminal substitution. Comparing the members of group a, per6benzester (**1a**), per6benzamide (**1b**), and per12benzamide (**4**), the liquid crystal to isotropic melting temperature decreased in going from the ester (257 °C for **1a**) to amide (216 °C for **1b**). When the flexibility was increased by increasing the length of the spacer segment connecting the perylenebisimide core to the terminal benzene unit from 6 to 12 alkyl units (**1b** and **4**), the melting temperature decreased still further to 206 °C. The liquid-crystal window increased from 18 °C for the ester **1a** to 41 °C for the longer spacer amide **4**. Although only one transition was observed in the cooling cycle of the spacer 12 amide, i.e., **4**, it remained frozen in the liquid-crystal phase until room-temperature upon cooling. A comparison of the members of group c, per6tridodecbenzester (**3a**), per6tridodecbenzamide (**3b**), and per12tridodecbenzamide (**5**), showed that the liquid crystal to isotropic melting transition decreased only very slightly in going from the ester **3a** (137 °C) to the amide **3b** (132 °C). It further increased to 173 °C upon the length of the flexible alkyl spacer segment being increased from 6 to 12 units in going from **3b** to **5**. The members of group b, per6dodecbenzester (**2a**) and per6dodecbenzamide (**2b**); contrary to the observation for the unsubstituted and tridodecyloxy-substituted benzene series, the melting transition was higher for the amide (249 °C) compared to the ester (229 °C). The members of this group had the largest liquid-crystal window among the whole series, which indicates the exceptional stability of the liquid-crystalline phase. This result is in agreement with the solution studies using UV−vis absorption spectroscopy, which established the formation of aggregates only for per6dodecbenzester (**2a**) in the ester series and aggregates of substantial stability having the highest transition temperature to the molecularly dissolved species for the corresponding per6dodecbenzamide (**2b**). The strongest hydrogen-bonding ability of per6dodecbenzamide (**2b**) was also confirmed by its having the highest melting transition temperature of 249 °C compared to those of **1b** (216 °C) and **3b** (132 °C).

X-ray diffraction measurements were performed on the ester series **1a**, **2a**, and **3a** as the pristine material and a film of the compound that had been heated above the melting point and cooled to room temperature.[38] The pristine powder material of per6benzester (**1a**) showed a large number of sharp reflections in the $2\theta$ range 3–35°, which increased in number and became sharper after heat treatment, indicating transition from one crystal form in the pristine material to another after heat treatment. The X-ray diffraction pattern of sample **1a** and a table giving the $d$ spacing values and their intensities for the three samples at room temperature and after heat treatment are given in the Supporting Information. Samples **2a** and **3a** remained frozen in the LC state upon cooling from the isotropic melt to room temperature; therefore, the XRD data after the heat treatment gives information regarding the LC phase. Figure 11a shows the X-ray powder diffraction data for the sample **2a** before and after heat treatment. It can be seen that after the heat treatment, a number of reflections in the wide-angle region have disappeared and a few sharp peaks have appeared in the small-angle region. The X-ray diffraction pattern after heat treatment showed a peak at $d = 13.48$ Å, with a second order of this reflection at $d = 6.74$ Å. Similarly, for the peak at $d = 20.22$ Å, there was a second-order reflection at $d = 10.11$ Å. The presence of these peaks is a strong evidence of a layered smectic structure in the LC phase of **2a**.[39] This is in accordance with the enthalpy of phase-transition data obtained from the DSC measurement. A small enthalpy value for crystal to LC transition followed by a large enthalpy value for LC to isotropic transition is indicative of an LC phase that is ordered more like that of a smectic phase. The X-ray diffraction pattern for the trialkoxy-substituted molecule **3a** showed a diffuse halo around $d = 4$–5 Å, which can be attributed to disordered alkyl chains.[19,37,38] In the small-angle region, it had one sharp scattering. After the molecule was cooled from the isotropic to room temperature, a comparatively sharp peak appeared in the wide-angle region corre-

(38) Debije, M. G.; Chen, Z.; Piris, J.; Neder, R. B.; Watson, N. M.; Mullen, K.; Würthner, F. *J. Mater. Chem.* **2005**, *15*, 1270–1276.
(39) Brochsztain, S.; Rodrigues, M. A.; Demets, G. J. F.; Politi, M. J. *J. Mater. Chem.* **2002**, *12*, 1250–1255.

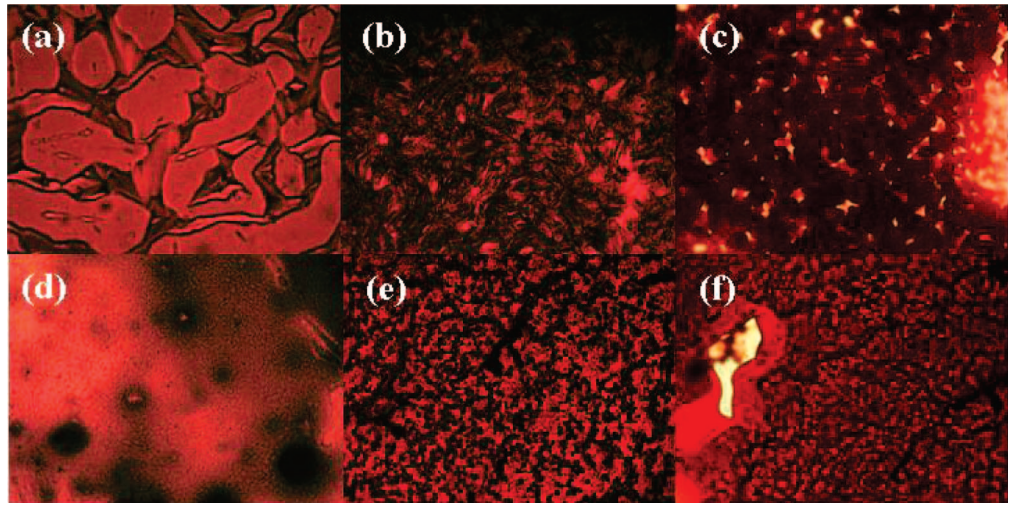


**Figure 10.** Polarized optical micrographs of the mesophase textures per6dodecbenzester **2a** at (a) 202 and (b) 64 °C, (c) per6tridodecbenzester **3a** at 98 °C, (d) per6dodecbenzamide **2b** at 198°C, and per6tridodecbenzamide **3b** at (e) 96 and (f) 42 °C.

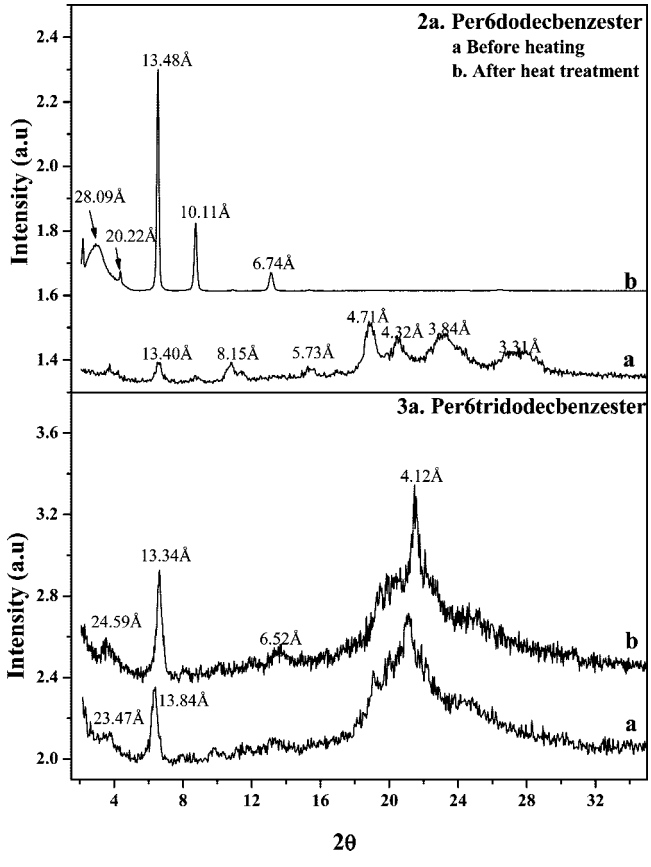


**Figure 11.** Powder X-ray diffraction data after heating above the clearing point and cooling to room temperature.

sponding to $d = 4.12$ Å. On the basis of similar results reported in the literature, it can be assumed that **3a** has a columnar LC phase with a periodicity of 4.12 Å (Figure 11b).[19,35] This $d$ value of 4.12 Å is characteristic of a close $\pi-\pi$ interaction of the perylene core in the system.

**Thin-Film Morphology.** Perylenebisimide derivatives have been shown to favor the formation of nanostructures along one dimension.[40] The effect of the functional group ester vs. amide and presence or absence of flexible alkyl terminal chains on the self-assembling properties of the perylenebisimide derivatives could be visualized from the scanning electron micrographs (SEM) of drop cast thin films from toluene. Thin films were fabricated by drop casting a $1 \times 10^{-5}$ M solution in toluene on to thin cover glass slides. These were subjected to solvent annealing by placing the films in a vacuum desiccator with a small vial of toluene also inside.[26,27] A slight vacuum was applied so as to saturate the desiccator with solvent vapor and then the films were left to anneal in the presence of the solvent for 12 hours. Such a solvent vapor annealing approach enables a slow molecular assembling process to take place that allows molecules to organize themselves into the most stable packing conformation. Finally, the films were removed from the desiccator and air-dried before the SEM measurements. Figure 12 showed the SEM images of self-assembled **1b**, **2b**, **3b**, and **2a** in toluene. From the electron micrograph image of per6benzamide **1b** (Figure 12a), we can see one-dimensional rodlike supramolecular structures with diameters in the range of 0.5–1.0 $\mu$m and lengths several micrometers long. These rods also tend to aggregate into bigger rods. The inset shows different regions of the same film showing clustered rods. Figure 12b showed the SEM images of per6dodecbenzamide (**2b**), which showed the maximum aggregation tendency in the solution studies. Supramolecular organization of rods stacked several micrometers long can be seen. In regions in which isolated rods could be identified, the thinnest rods had widths in the 150 nm range. The length is in the range of a few tens of micrometers, leading to aspect ratios (length over width) of magnitude 100. This long aspect ratio compared to that of the unsubstituted **1b** is consistent with the longer molecular length of **2b** with respect to **1b**. The inset shows an isolated rod 6 $\mu$m long having a diameter of 0.7 $\mu$m with well-defined sharp edges. The SEM image of per6tridodecbenzamide (**3b**) (Figure 12c), on the other hand, showed one-dimensional ball-like supramolecular structures having 3−4 $\mu$m diameters that are interconnected by nanometer-scale rods (indicated by arrows). The bulky tridodecyl substitution at the terminal benzene rings gives

(40) Li, Y.; Li, Y.; Li, J.; Li, C.; Liu, X.; Yuan, M.; Liu, H.; Wang, S. *Chem.—Eur. J.* **2006**, *12*, 8378–8385.

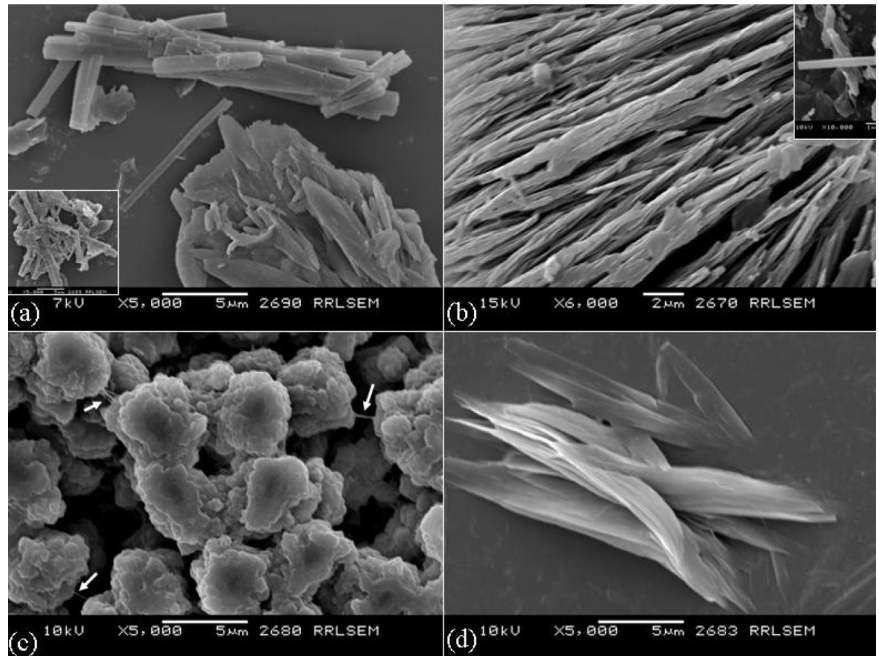


**Figure 12.** Scanning electron micrograph (SEM) images of self-assembled (a) per6benzamide **1b**, (b) per6dodecbenzamide **2b**, (c) per6tridodecbenzamide **3b**, and (d) per6dodecbenzester **2a** drop-cast from toluene.

rise to these larger spherical structures. Figure 12d shows the SEM micrograph of per6dodecbenzester **2a**, the only molecule in the ester series that showed an aggregation tendency in the solution studies. The leaflike pattern, which was 1.8−3 $\mu$m across in diameter and several micrometers long, was distinctly different from the rod- or ball-like aggregates formed by the amide series. The absence of an additional building force like that of the hydrogen-bonding force in the amide series results in a different morphology for the aggregated ester derivative, which has only $\pi-\pi$ interaction to aid in its self-assembly process.

## Conclusions

A new perylenebisimide amide and ester series were synthesized and their aggregation characteristics and phase behavior were investigated using a combination of UV−vis, fluorescence spectroscopies, differential scanning calorimetry, polarized light microscopy, and X-ray diffraction measurements. The comprehensive study reported here is an attempt at understanding some of the fundamental aspects like effect of functionalities like ester vs amide linkage, effect of length of alkyl spacer segment connecting core and terminal units, effect of presence or absence of long terminal alkoxy substituents, etc., on the aggregation behavior, packing in the solid state as well as the induction of thermotropic liquid-crystalline phases in a series of perylenebisimides. It has shown some understanding of the effects of subtle differences in substitution strategy on the aggregation geometry driving the formation of J or H type of packing. The study has indicated, quite unexpectedly, that the presence of a single terminal dodecyloxy phenyl substituent has a very stabilizing effect on the overall properties like stability of liquid-crystalline phases, stability of aggregates formed, etc., when compared to no terminal dodecyloxy benzyl substitution or tridodecyloxy benzyl substitution. This was true for both the ester as well as amide linkage having monododecyloxy benzene substitution. Furthermore, the SEM images indicated that well-defined structures could be fabricated by self-assembly induced by the $\pi-\pi$ interaction of the perylenebisimide core and the hydrogen-bonding interaction. We have thus successfully showed that suitable design strategies like combination of supramolecular hydrogen-bonding interactions and liquid-crystalline ordering can be used to obtain better organization in perylenebisimide derivatives, which can find possible applications as electron-accepting materials in organic photovoltaic solar cell devices.

**Acknowledgment.** The authors thank the DST Fast Track Scheme for Young Scientists (Project SR/FTP/CS-33/2004) and KSCTSE, Thiruvananthapuram, Kerala, India (No. 030/SRSPS/2005/CSTE) for supporting this research. We thank Dr. Peter Koshy and Mr. M. R. Chandran, RRL-Trivandrum, for the SEM analysis and Dr. U. Syamaprasad and Mr. P. Gurusamy, RRL-Trivandrum, for XRD analysis. We also thank the sophisticated analytical instrument facility in the Central Drug Research Institute, Lucknow, for the MALDI-TOF analysis. Thanks are also due to CSIR, New Delhi, for financial support to J.B.

**Supporting Information Available:** SEC plot, MALDI-TOF spectra, $^1$H NMR spectra, UV−vis spectra, X-ray diffraction data, SEM images, and TGA plot (PDF). This material is available free of charge via the Internet at http://pubs.acs.org.

CM702497Y